Desalination and Water Treatment
www.deswater.com
doi: 10.5004/dwt.2020.26286

204 (2020) 93–106
November

Mixed matrix polyethersulfone tight ultrafiltration (TUF) membrane with improved dye removal by physical blending of 2D MoS_2

Huali Tian[a,b], Xing Wu[c], Kaisong Zhang[a,*]

[a]*Key Laboratory of Urban Pollutant Conversion, Institute of Urban Environment, Chinese Academy of Sciences, Xiamen 361021, China, emails: kszhang@iue.ac.cn (K. Zhang), hltian@iue.ac.cn (H. Tian)*
[b]*University of Chinese Academy of Sciences, Beijing 10049, China*
[c]*CSIRO Manufacturing, Clayton South, Victoria 3169, Australia, email: Xing.Wu@csiro.au (X. Wu)*

Received 6 January 2020; Accepted 16 June 2020

ABSTRACT

Tight ultrafiltration (TUF) membrane as a kind of ultrafiltration membrane has great promising applications in wastewater treatment and molecule separation. We report a facile and scalable technique for the fabrication of mixed matrix TUF membrane by physical blending of two-dimensional (2D) molybdenum disulfide (MoS_2) with polyethersulfone dope solution. The incorporated MoS_2 sheets affected the phase inversion process and changed the membrane structure. Morphology, molecular weight cut-off, hydrophilicity, and mechanical strength properties of the prepared membranes were investigated. The characterization by field emission scanning electron microscopy confirmed that MoS_2 sheets were successfully embedded in the membranes and transmission electron microscopy confirmed the well-distribution of MoS_2 in the membrane matrix. Results demonstrated that the pore size of membranes was effectively tailored by varying the content of MoS_2 from 0 to 5.0 wt.% in casting solutions. The modified TUF membranes with MoS_2 concentration in the range of 2.5–4.0 wt.% showed an enhanced pure water flux and higher polyethylene glycol (PEG, 10 kDa) rejection compared to the pristine membrane. An optimized pure water flux of 84.7 L m^{-2} h^{-1} bar^{-1} and a superior PEG 10 kDa rejection of 95.2% were obtained for the membrane modified by MoS_2 sheets with a concentration of 3.0 wt.%. Moreover, the as-prepared TUF membrane showed 91.6% rejection rate for a small molecule (rose bengal, 1,017 g mol^{-1}), indicating their narrow pore size. This work has highlighted the facile physical blending of MoS_2 and polymeric dope solution, thus providing a promising application for other polymeric ultrafiltration membranes.

Keywords: Tight ultrafiltration membrane; Molybdenum disulfide; Two-dimensional nanomaterial; Polyethersulfone

1. Introduction

Ultrafiltration membrane (UF) has been extensively applied for separation and product recycling such as protein, fruit juice, and oil–water [1]. However, the pore sizes of most of UF membranes are approximately between 10 and 100 nm, which results to the ineffective removal of pollutants with a size smaller than 10 nm such as organic micropollutants (including dyes, antibiotics, pesticides, and natural organic matter (NOM)) [2,3]. To overcome this limitation, tight ultrafiltration (TUF) membranes with a smaller pore size (approximately molecular weight cut-off (MWCO) 1,000–10,000 Da) has been proposed in recent studies [4,5]. Several works have been conducted to examine the feasibility of TUF membranes for the treatment of various organic waste and wastewater such as landfill leachate [6], food waste [7,8], textile wastewater, and dye/salt liquids wastes [9]. However, compared to ordinary UF membranes, the water flux of current TUF membranes is relatively low, which leads to higher energy consumption in the separation

* Corresponding author.

process [10]. The performance of UF membranes is usually determined by the pore size of membranes. Therefore, it is critical to explore the strategies for fine-tuning the pore size to enhancing the permeability of TUF membranes without compromising the rejection property.

Polyethersulfone (PES) has excellent thermal stability (T_g = ~225°C), high mechanical behavior, and good chemical resistance. It is one of the most common polymer materials for the preparation of UF membranes [11–13]. In order to prolong the membrane life and reduce the manufacturing costs, modification methods such as blending, surface modification, and bulk modification are used to improve permeability, selectivity, and antifouling of the membrane [14]. Usually, the blending technique is relatively simple to operate and only requires mild preparation conditions [15]. Blending with inorganic nanomaterials to fabricate a mixed matrix membrane was one of the effective methods used in improving the membrane performance [16,17]. This improvement can be attributed to the two following effects, first, incorporating an inorganic ingredient into a polymer matrix to form a new material having expectedly the best properties of each material. Another reason is that the presence of nanoparticles in dope solutions affect thermodynamically and rheologically, change the phase transition mechanism when preparing a nanocomposite membrane by phase inversion method [18]. A variety of nanomaterials have been introduced into PES matrix to prepare high-performance new membrane, such as silver [19], carbon nanotube [20], TiO_2 [21,22], GO [23,24], and so on.

Molybdenum disulfide (MoS_2) is one type of 2D materials, which is one of the most studied transition metal dichalcogenides (TMDCs) [25]. A single-layer MoS_2 has a thickness of ~1.0 nm, and has a sandwich-like structure consisting of two atomic planes of S and one atomic plane of Mo. The existing nanopores and interlayer channels, potentially create transport channels for gas or water molecules. MoS_2 membranes have been applied for H_2/CO_2 separation [26], desalination [27–29], and dye removal [30]. It was recently reported that the water flux performance of MoS_2 porous membranes performs better than the graphene nanopore membranes recording up to 70% efficiency [27]. However, membrane fabricated by MoS_2 faces several challenges during industrial production. For example, current MoS_2 membranes are usually prepared by using single-layered or few-layered MoS_2, which requires complex chemical modification process or high-energy exfoliation. Moreover, the membrane size of MoS_2 membranes is also limited [31]. Doping commercial MoS_2 nanoparticles in a casting polymer solution and synthesizing the membrane through phase inversion provides a new strategy for utilizing MoS_2 in polymeric membranes. Compared to the complicated chemical functionalization or time-consuming pre-treatment for MoS_2 membranes, physical blending by commercial MoS_2 was considered to be more reliable and suitable for scale due to its simplicity, green, and low cost [32,33].

Herein, a series of PES/MoS_2 mixed matrix TUF membranes with MWCO less than 10 kDa were prepared and investigations were carried out by fine-tuning the membrane pore sizes using varying concentrations of commercial MoS_2. Meanwhile, for the first time, we investigated the influence of the amount of MoS_2 sheets on the structure of the TUF membranes. By optimizing the loading of MoS_2, both the pure water flux and the rejection performance of TUF membranes were significantly enhanced, implying a potential breakthrough for the trade-off between the permeability and selectivity property of membranes. Moreover, the recorded water flux of PES/MoS_2 TUF membranes in this study was higher than TUF membranes with similar MWCO in other studies. Thus, this work introduces a facile and scalable method to fabricate PES/MoS_2 mixed matrix TUF membranes, which can perform well in continuous or batch operation, and entirely suitable for industrial application.

2. Experimental

2.1. Materials

Commercial PES (Ultrason E6020P, Mn = 52,000 g/mol) was purchased from BASF, Germany. Before use, PES was dried overnight in a 105°C vacuum oven. MoS_2 (99.5% metals basis, <2 μm, Aladdin, China), *N*,*N*-dimethylacetamide (DMAc) was bought from Shanghai Jinshan Jingwei Chemical Co., Ltd., (China). Polyvinylpyrrolidone (PVP K30), polyethylene glycol (PEG, 2,000; 4,000; 6,000; 8,000; and 10,000 Da), rose bengal (MW1017.64 Da) and direct red 80 (1373.07 Da) were acquired from Sigma Aldrich (Germany). Deionized (DI) water was used in all experiments.

2.2. Preparation of membranes

The casting solutions were prepared according to the compositions given in Table 1. Different concentrations of dry MoS_2 were added to the DMAc solution and sonicated for 4 h to make it well-dispersed. Then PVP and PES were dissolved in the solvent and stirred at 60°C until a uniform casting solution was obtained. The casting solution was kept in an oven at 60°C overnight to completely remove air bubbles. To fabricate the membrane, the casting solution was dripped on a piece of non-woven fabric and was cast using a casting knife gap setting of 200 μm at ambient temperature. After casting, the non-woven fabric was immersed into a DI water bath immediately. Finally, the prepared membrane was transferred into fresh pure water for 24 h to remove residuals then stored in DI water before using.

2.3. Membrane characterization

To verify the existence of MoS_2 in the PES/MoS_2 membranes, surface enhanced Raman scattering spectra were acquired using a Lab-RAM Aramis (HORIBA Jobin Yvon) confocal micro-Raman system. X-ray diffraction (XRD) patterns of the prepared samples were measured using X'Pert PRO at a scanning rate of 10°min^{-1} in the range of 10°–70°. The structures of surface and cross-section of membranes were observed by field emission scanning electron microscopy (FE-SEM, HITACHIS-4800, Hitachi, Japan) at an acceleration voltage of 5.0 kV at various magnifications. Before FE-SEM observation, membrane samples were sputtered with gold. A further observation of the cross-sections of membranes was obtained by transmission electron microscopy (TEM, H-7650, Hitachi, Japan) analyzing. Membrane samples were dried, and then placed in a

Table 1
Blend composition of mixed matrix PES/MoS_2 membranes

Membrane	PES (wt.%)	PVP (wt.%)	DMAc (wt.%)	MoS_2 (wt.%)	Viscosity (mpas)
M0	23.0	16.0	61.0	0.0	74,000 ± 173.21
M1	23.0	16.0	59.0	2.0	93,133.33 ± 152.75
M2	23.0	16.0	58.5	2.5	102,400 ± 624.50
M3	23.0	16.0	58.0	3.0	115,200 ± 624.50
M4	23.0	16.0	57.0	4.0	113,366.67 ± 776.75
M5	23.0	16.0	56.0	5.0	126,800 ± 692.82

spur resin for 36 h at 35°C. Samples were transferred to flat embedding molds filled with fresh resin and polymerized for 24 h at 70°C. Leica UC7 ultra-thin slicer was used to cut the samples into 100 μm ultrathin sections, and then dried the slices. Images were obtained with a TEM [34] and analyzed with the software Image J to determine the distribution of MoS_2 in membranes [35]. The surface roughness of membranes was determined with atomic force microscopy (AFM, Bruker-Dimension Edge, USA). The hydrophilicity of the membranes was measured using a contact angle goniometer (CA, DSA100, KRUSS, Germany). Average contact angle values were obtained by measuring each sample at three different locations. The mechanical property of prepared membranes was evaluated by using tensile testing equipment (NTS, LRK-500N). The membrane was initially fixed at a distance of 55 mm with grips, and then the movable crosshead with a 500 N load cell was used to pull the membrane at a constant rate of 100 mm min^{-1} until the membrane was broken.

2.4. Evaluation of membrane properties

The MWCO, the pore size, and pore size distribution of TUF membrane were tested by filtrating different molecular weights of PEG (2,000; 4,000; 6,000; 8,000; and 10,000 Da). The test was performed using a dead-end filtration cell (Model 8010, Millipore Corp., USA) at room temperature (25°C ± 1°C). An effective membrane area of 4.1 cm^2 was used for the filtration process at 0.1 MPa and 1.0 g L^{-1} PEG solution was used as the feed liquid. The concentration of the feed and permeate solution was tested by a total organic carbon analyzer (TOC, TOC-LCSH, Shimadzu, Japan), respectively [36]. The MWCO of the membranes was defined using the different PEG retained at 90% [37]. The PEG rejection was calculated using Eq. (1):

$$R(\%) = \left(1 - \frac{C_p}{C_f}\right) \times 100 \tag{1}$$

where C_p is the concentration of the permeate solution and C_f is concentrated concentration of the separation solutions.

It has been reported that the mean effective pore size (μ_p) of the membrane equals to the stokes diameter (d_s) of PEG at 50% rejection, and the stokes diameter (d_s) can be calculated using Eqs. (2) and (3) [38]:

$$r_s = 16.73 \times 10^{-12} \times M_{\mathrm{PEG}}^{0.557} \tag{2}$$

$$d_s = 2 \times r_s \tag{3}$$

where r_s is the stokes radius and MPEG is the molecular weights of PEG.

To determine the pore size distribution, the geometric mean diameter (μ_s) and geometric standard deviation (σ_g) of the membrane was taken into consideration. The geometric mean diameter (μ_s) can be calculated as d_s corresponding to R = 50%, while the geometric standard deviation (σ_g) can be determined from the ratio of d_s at R = 84.13% and 50%. By ignoring the dependence of solute separation on the steric and hydrodynamic interaction between solute and pore sizes, the mean effective pore diameter (μ_p) and the geometric standard deviation (σ_p) of the membrane can be considered to be the same as the value of μ_s and σ_g, respectively. Hence, the pore size distribution of the membrane can be mathematically fitted by the following probability density function [39,40]:

$$\frac{dR(d_p)}{dd_p} = \frac{1}{d_p \ln \sigma_p \sqrt{2\pi}} \exp\left[\frac{\left(\ln d_p - \ln \mu_p\right)^2}{2\left(\ln \sigma_p\right)^2}\right] \tag{4}$$

where d_p is the pore size of the membrane.

The membrane porosity ε (%) is defined as the ratio of the volume of the pores to the total volume of the membrane, which is determined by a gravimetric method [41]:

$$\varepsilon(\%) = \frac{\left(W_w - W_d\right)/D_W}{\left(W_w - W_d\right)/D_W + W_d/D_P} \times 100\% \tag{5}$$

where ε is the porosity of membranes (%), W_w is the wet weight of the membrane (g), W_d is the dry weight of the membrane (g), D_w (0.998 g cm^{-3}) is the density of the water, and D_p (0.37 g cm^{-3}) is the density of polymer.

2.5. Filtration performance of membranes

The water flux was measured by the same dead-end filtration system. Three membrane samples were prepressed at 0.15 MPa for 30 min. After prepressing, the permeate weight was recorded by an electronic balance at 0.1 MPa. The permeate flux (J_0) was calculated with Eq. (6):

$$J_0 = \frac{\Delta V}{A_m \Delta t} \tag{6}$$

where J_0 (L m^{-2} h^{-1}) is the membrane flux, ΔV (L) is the volume of permeated water, A_m (m^2) is the membrane area, and Δt (h) is the permeation time.

To investigate the long-term stability of TUF membrane, the modified membrane M3 (3.0 wt.% MoS_2) was tested with DI water at a pressure of 1.0 bar for 20 h. Collect concentrated water and permeated water every two hours to measure the concentration of the loss MoS_2. Before that, the MoS_2 was dispersed in water at a known concentration (0, 2.0, 4.0, 6.0, 8.0, 10, 12, and 20 mg L^{-1}) to draw a standard curve. The absorbance was measured by ultraviolet visible (UV-vis) spectrophotometer (Spectra Max M2, Molecular).

To investigate the rejection property of TUF membranes, varied feed solutions including PEG 10 kDa, rose bengal, direct red 80, and dye solutions with different concentrations (10, 50, and 100 mg L^{-1}) were applied. The concentration of dye was measured by UV-vis. The permeation flux (J) and rejection (R) of the dye were calculated by Eqs. (1) and (6), respectively.

2.6. Anti-fouling performance measurement

The permeation flux of water and pollutants alternate cycle was used to investigate the anti-fouling performance of the membranes. The stable value of pure water flux (J_{wi}) was recorded for 60 min. PEG 10 kDa (1.0 g L^{-1}) and rose bengal (50 mg L^{-1}) solution were applied as feed solution for another 60 min, respectively. The permeation flux of the PEG 10 kDa and rose bengal solution was recorded as (J_{pi}). The "i" was the cycle time. Then, the filtrated membrane was immersed in DI water and washed for 30 min. A new pure water flux of this membrane was recorded as J_{wi+1} in another 60 min. It presented one filtration cycle has competed. The flux recovery rate (FRR$_{ist}$), the total fouling rate (R_{ti}), the irreversible fouling rate (R_{iri}), and the reversible fouling rate (R_{ri}) were calculated with Eqs. (7)–(10), respectively.

$$\mathrm{FRR}_{ist}\,\% = \left(\frac{J_{wi+1}}{j_{wi}}\right)\times 100 \tag{7}$$

$$R_{ti}\ \% = \left(\frac{J_{wi} - J_{pi}}{j_{wi}}\right)\times 100 \tag{8}$$

$$R_{iri}\,\% = \left(\frac{J_{wi} - J_{wi+1}}{j_{wi}}\right)\times 100 \tag{9}$$

$$R_{ri}\ \% = \left(\frac{J_{wi+1} - J_{pi}}{j_{wi}}\right)\times 100 \tag{10}$$

3. Results and discussion

The morphology of MoS_2 (after 4 h of sonication) and MoS_2/PES membranes were observed by TEM images (Fig. 1). It could be observed from Figs. 1a–c that the MoS_2 shows a distinct lamellar morphology and the lateral size of

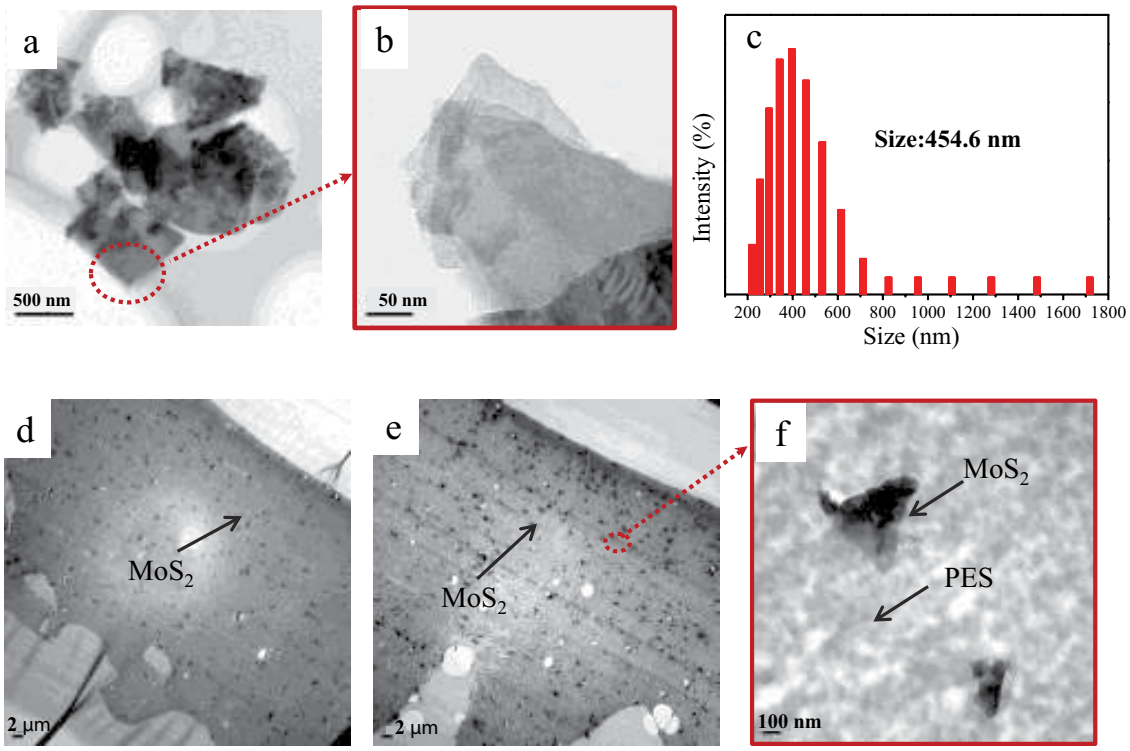

Fig. 1. TEM image of few-layer MoS_2 (a), lamellar morphology of MoS_2 (b), particle size distribution (c), cross-sectional TEM images of the M3 membrane (d), cross-sectional TEM images of the M5 membrane (e), and TEM images of few-layer MoS_2 in PES/MoS_2 membrane (f).

MoS_2 was around 450 nm. Figs. 1d and f exhibit that MoS_2 were successfully embedded and dispersed evenly in the PES matrix of the M3 and M5 membranes. A high-resolution TEM image (Fig. 1f) indicated that MoS_2 were bonded with the polymer firmly. The loading of MoS_2 in the M3 and M5 membranes was roughly analyzed through Image J software by comparing the area of MoS_2 and the total membrane area shown in TEM images. Fig. 2 shows that the total loading of MoS_2 in the M3 was 2.9% and in the M5 was 4.7%. In the M3 membrane, MoS_2 in the top-section was 2.4%, the middle-section was 2.9%, and the bottom portion was 3.9%. In the M5 membrane, the MoS_2 in the top-section accounted for 7% and the loading in the middle portion was 2.9% and in the bottom portion was accounted for 4.6%. The result indicated that MoS_2 were more evenly distributed in the M3 membrane. The MoS_2 tended to aggregate at excessive loading. Fig. 2 shows the obvious sheet agglomeration in the upper portion of the M5 membrane. Thus, the higher loading was not desirable.

Raman spectra of MoS_2 powder, PES membranes, and PES/MoS_2 membranes are depicted in Fig. 3a. In comparison with the M0 membrane, three new characteristic peaks appeared at 378, 402, and 452 cm^{-1} on the curve of the M3 membrane, which were associated with the existence of MoS_2 materials [42,43]. The crystallinity of the controlled M0 membrane and PES/MoS_2 membranes were characterized by XRD as shown in Fig. 3b. The peaks and high intensity from XRD were associated with the crystallinity of the material. All the membranes showed peaks in 2θ at 17.6°, 22.6°, and 25.9°, indicating the amorphous region of PES [44]. Compared to the M0 membrane, there were new peaks in the PES/MoS_2 membrane (M3). Peaks at 14.3°, 29°, 39.6°, 44°, 49.8°, and 60.1° were associated with MoS_2 sheets, which can be assigned to (002), (004), (103), (104), (105), and (110) planes, respectively [45,46]. These results revealed that MoS_2 had been successfully blended in PES/MoS_2 membranes.

The morphology of membranes was investigated by SEM as illustrated in Fig. 4. The influence of added MoS_2 on the casting solution could be noticed with increasing concentration of MoS_2 on the photograph of the fabricated membranes. During the phase inversion process, the MoS_2 migrated from PES matrix to the water bath and exposed on the membrane surface. By observing the top surface of membranes, it could be found that the unmodified membrane had a smooth surface. By adding MoS_2 into the casting solution, the surface roughness of the M3 and M5 membranes increased which was due to the existence of MoS_2 on the membrane surface.

The casting solution in this work contained 23 wt.% of PES, 16 wt.% of PVP. The role of PVP in the as-prepared casting solution was to adjust pore size and porosity. Although a small amount of PVP is commonly used as pore-forming agent in membrane fabrication, nevertheless, it has also been reported that higher concentration of PVP can decrease the macro-porosity of membranes [47,48]. Therefore, it could be observed that the M0 membrane was full of spongy-like structures, which was not the case in PES/MoS_2 membranes. The finger-like microvoids structures observed in PES/MoS_2 membranes were due to the presence of MoS_2 in the casting solution. The phase inversion mechanism of thermodynamics and rheology can be influenced by the presence of nanoparticles in the casting solution. With the different concentrations of nanoparticles, the phase inversion mechanism would be changed [49]. With the increase of MoS_2 load, the spongy-like structures of the membrane become denser, as shown in the enlarged view of the internal structure of the section. The commercial MoS_2 has a contact angle

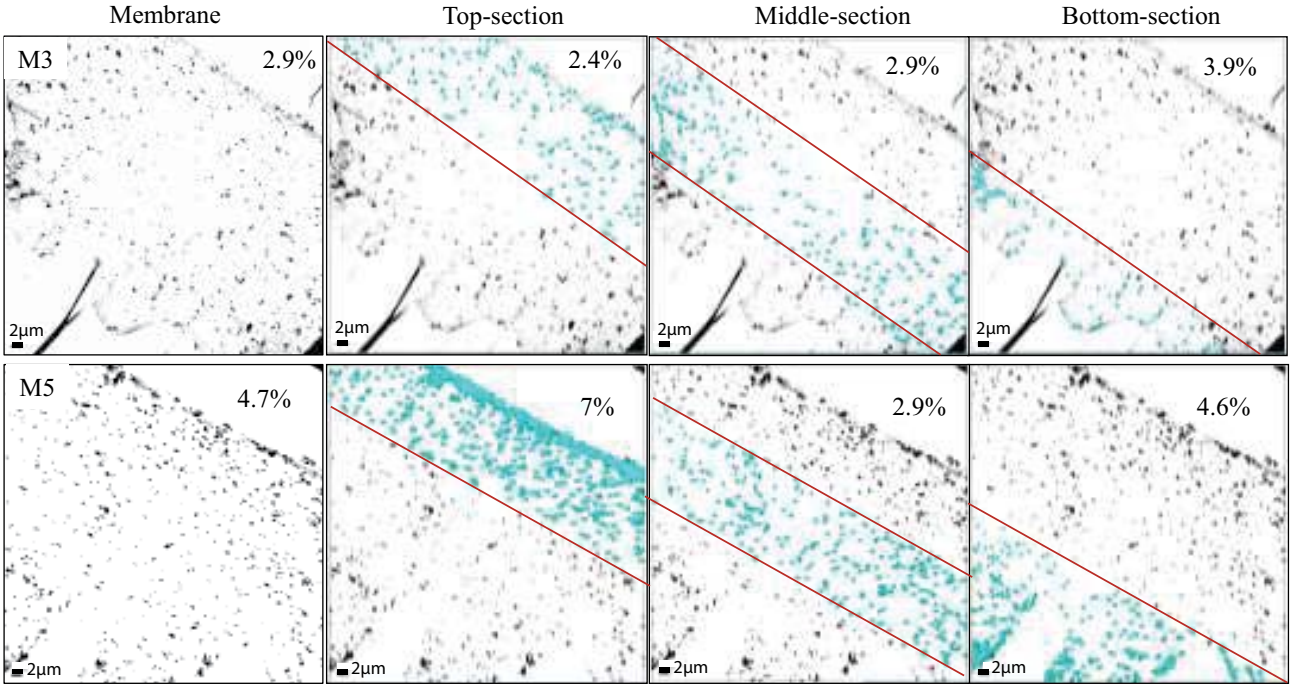

Fig. 2. With 8-bit format converted cross-sectional TEM images of the M3 and M5 membranes (Figs. 1d and e) and its equivalent drawings for calculation of MoS_2 area fraction in the top, middle, and bottom of the membrane.

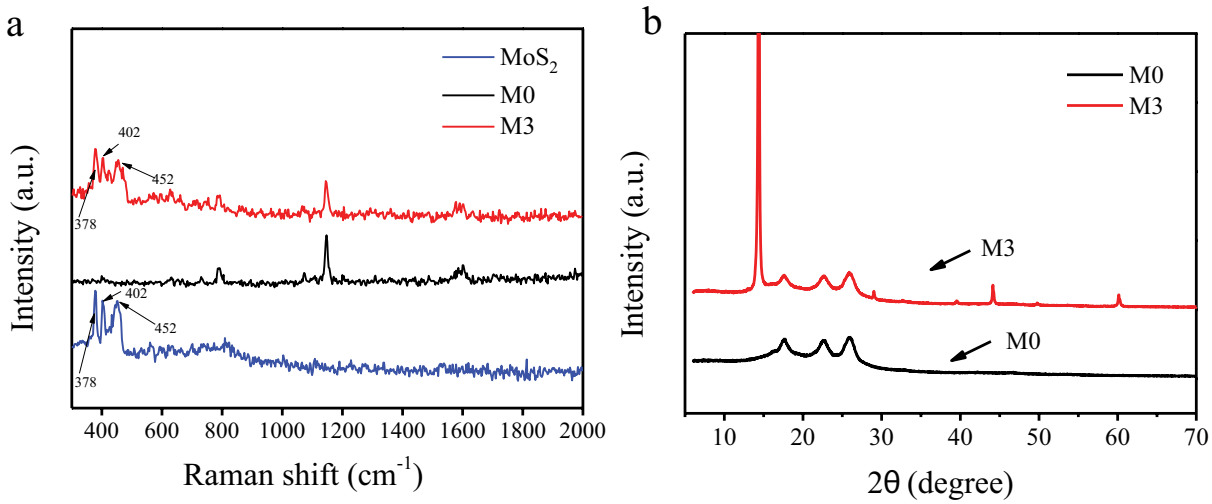

Fig. 3. Raman spectra of MoS_2, PES, and PES/MoS_2 membrane (a) and XRD patterns of PES membrane and PES/MoS_2 membrane (b).

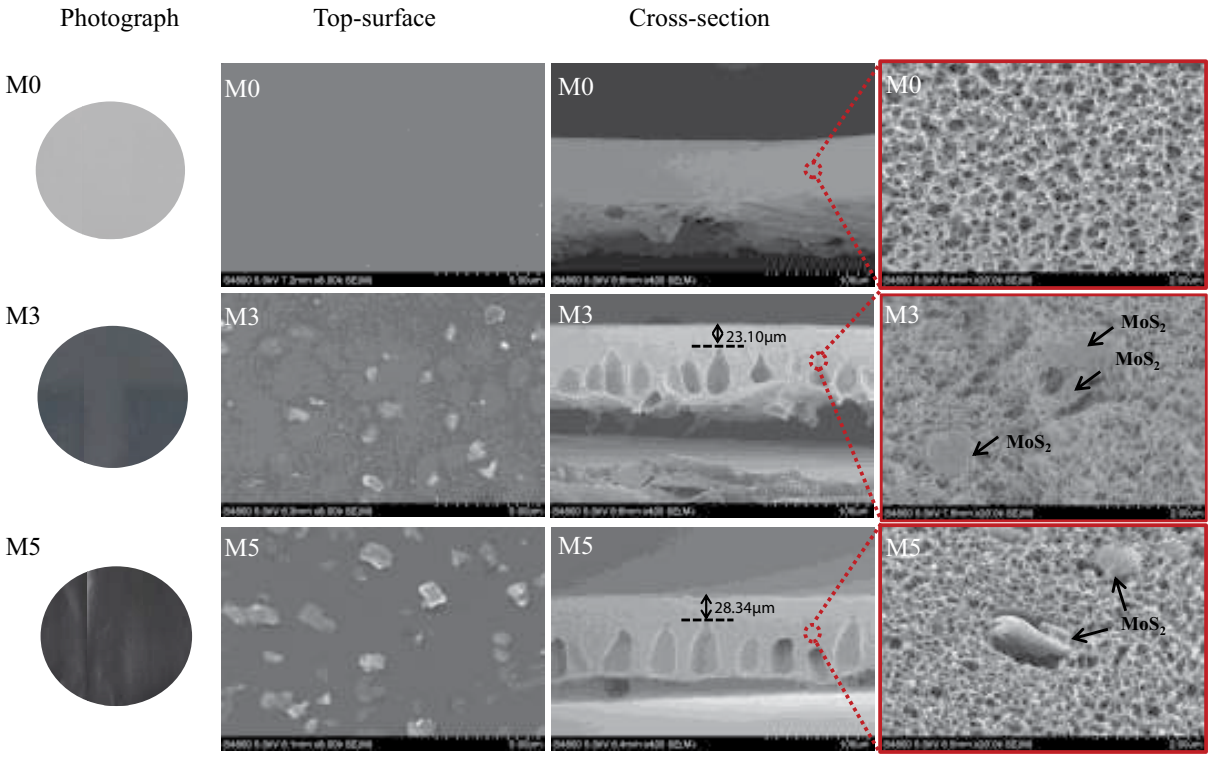

Fig. 4. SEM images of the surface and cross-sectional of PES and PES/MoS_2 Membranes.

of 80.2° ± 2.3°, which belongs to hydrophilic additive. The addition of MoS_2 increases the diffusion rate between solvent and non-solvent, increases the phase separation velocity, thereby, promoting the formation of finger-like macro voids in the sub-layer [50]. As shown in Fig. 4, the macro voids of M3 were closer to the skin layer. However, when containing a higher content of MoS_2 (5.0 wt.%), a relatively serious aggregation of MoS_2 occurred in the polymer matrix of the M5 membrane. The agglomeration of MoS_2 sheets would block the pores and make the water flux reduced. When the content of MoS_2 sheets was 5.0%, the high viscosity delayed phase inversion, resulting in the dense membrane and the macro voids move away from the dense skin layer.

The AFM was used for further analysis of membrane surface roughness. The 3D images scanning area of 10 μm × 10 μm are shown in Fig. 5. Result indicated that the M0 membrane displayed a smooth surface with an average roughness (R_a) value of 3.44 nm. However, the presence of MoS_2 in PES/MoS_2 membranes created rougher surfaces, and the roughness increased with the concentration of MoS_2.

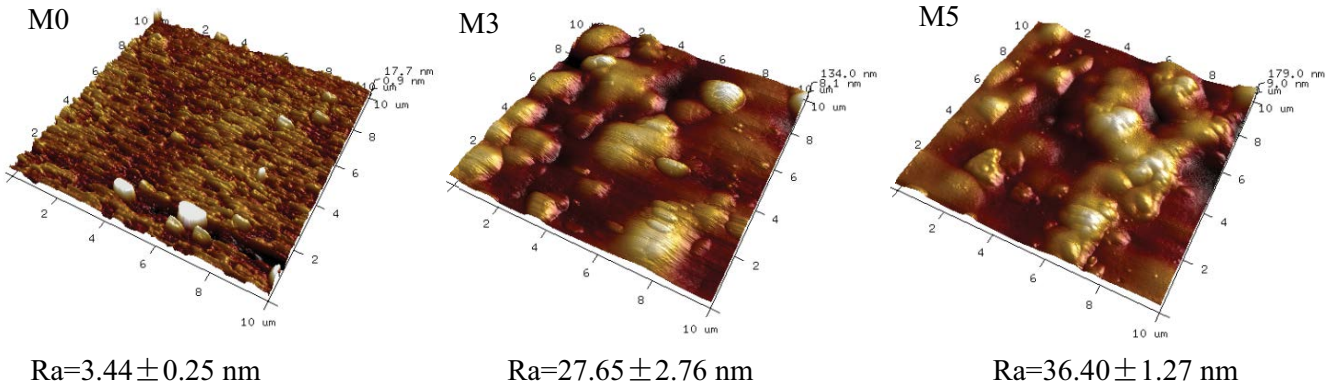

Fig. 5. AFM images of the M0, M3, and M5 membranes.

The increase of membrane surface roughness was consistent with the observation of SEM. The increase of surface roughness led to the increase of effective filtration area, which could be good to improve permeation performance.

The water contact angle was measured to investigate the hydrophilicity of as-prepared TUF membranes. The contact angle of MoS_2 was 80.2° ± 2.3° (77.7°–83.3°). When blending with PES and PVP, MoS_2 changed the hydrophilicity properties of the membrane. The control membrane was approximately 58.5° ± 2.1°as shown in Fig. 6a. The CA values of the composite membranes rose gradually M1 = 71.8° ± 0.8°, M2 = 75.1° ± 2.0°, M3 = 78.3° ± 1.3°, M4 = 79.3° ± 1.4°, and M5 = 79.1° ± 1.2° with the increase in the concentration of MoS_2.

Tensile strength and elongation at break were tested to represent the mechanical strength properties of fabricated membranes. It can be observed from Fig. 6b that the tensile strength of the M0 membrane was 42.85 MPa and the elongation at break was 8.17%. By blending 3.0 wt.% of MoS_2, the M3 membrane showed an increase in tensile strength (56.32 MPa) and the elongation at break (10.55%). This result confirmed that a moderate content of MoS_2 can improve the mechanical strength of membranes, which was in line with other studies about MoS_2 mixed matrix membranes [51]. In the mixed matrix membrane, MoS_2 sheets can be well compounded with the PES matrix, which increased the rigidity of polymeric chains and consequently improved the mechanical strength of mixed matrix membranes. However, the M5 membrane has lower tensile strength compared to the M0 and M3 membranes which were potentially due to the poor dispersibility of MoS_2 sheets in the M5 membrane. As shown in Figs. 1e and 2 (M5) the relatively worse-dispersive MoS_2 sheets in the M5 membrane potentially caused the aggregation of sheets and created more defects in the membrane. Moreover, cavities between the MoS_2 sheets and the polymer matrix were relatively enlarged when the concentration of MoS_2 increased to 5.0 wt.%, as shown in Fig. 4. Therefore, the tensile properties of the hybrid membrane were weakened. Another major reason for the reduced tensile strength of the M5 membrane was associated with the longer and wider finger-like structure in the membrane [52].

As shown in Fig. 7, the fabricated membranes exhibited different MWCO, ranging from 8.69 to 9.77 kDa, which indicated that these membranes were TUF membranes [53]. The pore size of membranes was effectively tailored between 3.45 and 3.87 nm by varying the content of the

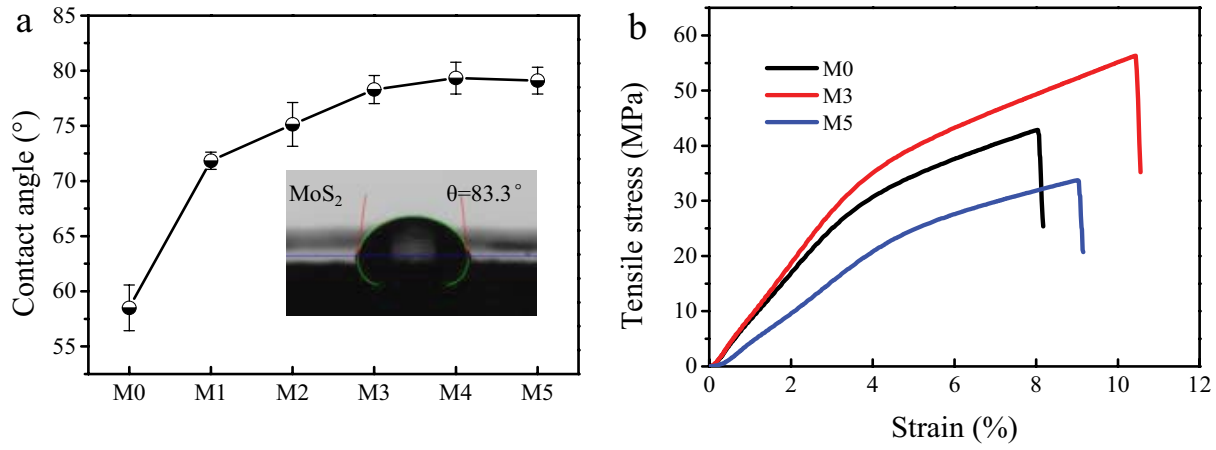

Fig. 6. Pure water contact angles of PES and PES/MoS_2 membranes (a) (insert figure show contact angle of MoS_2), stress–strain behaviors of M3, and M5 membranes (b).

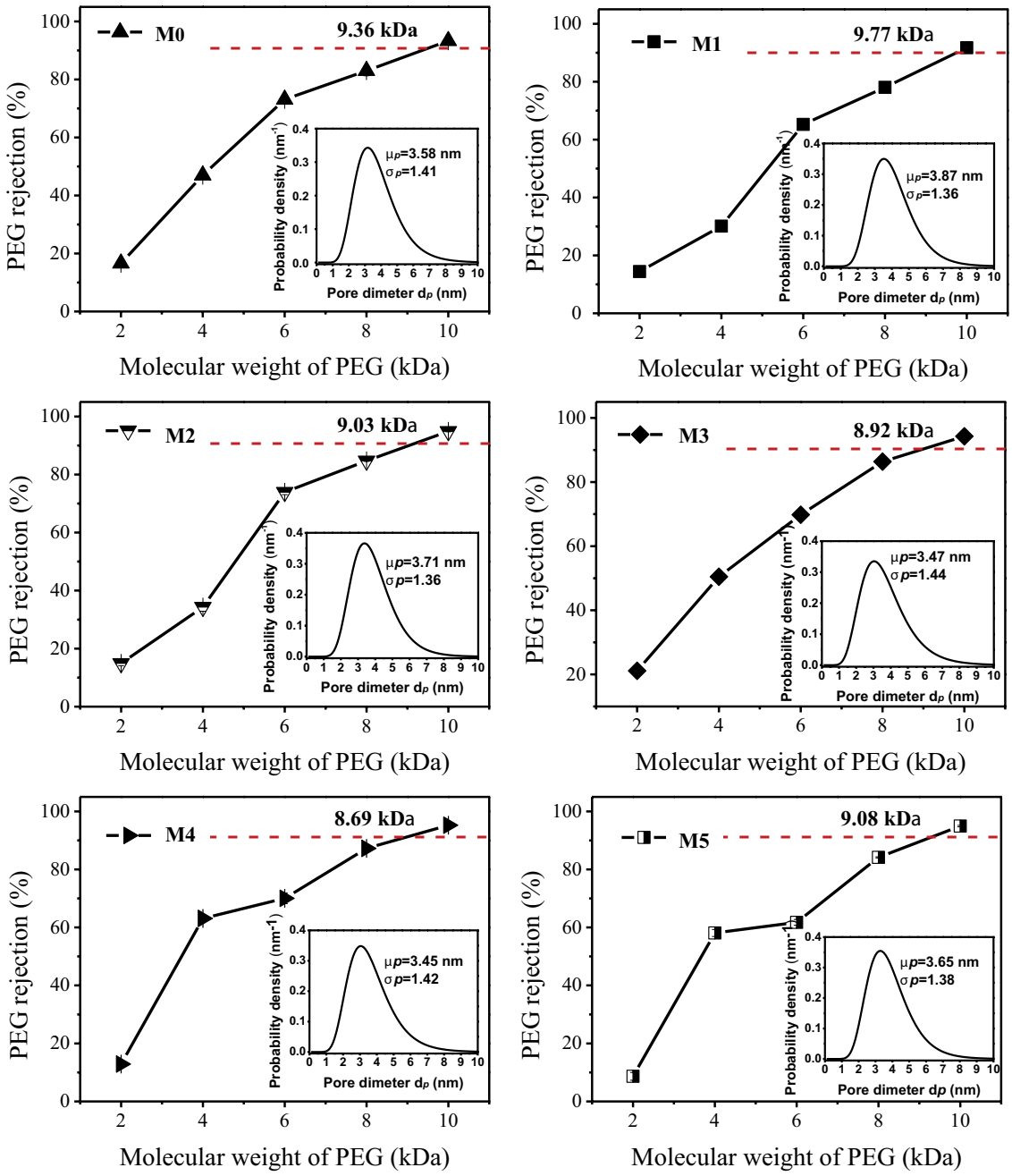

Fig. 7. MWCO and pore size distribution (insert figure) of membranes.

two-dimensional (2D) MoS_2 (0–5.0 wt.%). In general, with a decrease of MWCO, the pore radius declines. It can be observed that the mean effective pore size (μ_p) and the MWCO of the M1, M2, M3, and M4 membranes dropped gradually when the concentration of fillers increased from 2.0% to 4.0 wt.% [54,55]. However, when compared to the M0 membrane, the M1 and M2 membranes had larger pore sizes, while MWCO variation trends were different. This is probably because in the MoS_2/PES mixed matrix membrane, the free volume cavities in polymer chains, the organic–inorganic network structures, and the interlayer galleries between MoS_2 produced the molecules transfer channels [56]. When the content of MoS_2 was 2.0 wt.%, the MoS_2 dispersed uniformly in the interior of the membrane matrix, disturbed the PES chains, and increased the free volume cavities. These transport channels were more conducive to PEG molecules through the membrane. When the content of MoS_2 was 2.5–4.0 wt.%, the MWCO reduced from 9.77 kDa (M1) to 8.69 kDa (M4), the pore size reduced from 3.87 nm (M1) to 3.45 nm (M4). These are probably attributed to the compact organic–inorganic network structures and the number of interlayer galleries

increased (Fig. 4, M3). In addition, the presence of two different atoms, Mo and S, in MoS_2, increasing the flexibility of organic–inorganic network structures in the membrane [57]. On the other hand, when the amount of MoS_2 sheet was added, some of them form on the surface, MoS_2 stack in a disordered manner and construct transfer channels [58]. By further increasing the amount of MoS_2 sheet in casting solutions, the M5 membrane had a larger pore size and higher MWCO compared to the M4 membrane. This might be as a result of the aggregation of MoS_2 in the inner membrane and membrane surface. Another influence of MoS_2 on the structure of the membrane is the reduced porosity of membranes. The porosity of the M0 was 54.54% ± 0.78%. The porosity of the M1 membrane fell to 50.94% ± 0.87%. With the increase of MoS_2 loading, the porosity of the membrane decreased gradually and the M5 membrane showed that the porosity reduced up to 46.79% ± 1.12% with blending 5.0 wt.% MoS_2.

The pure water flux and PEG 10 kDa rejection properties of the fabricated TUF membranes were investigated, and the results are displayed in Fig. 8. The pristine membrane with MWCO of less than 10 kDa (pore size 3.58 nm) and a high water flux (76.16 L m^{-2} h^{-1}) was prepared. Compared to other solvents used for the preparation of similar membranes, such as Alibakhshi et al. [59] reported that *N*-methyl pyrrolidone (NMP) could be an appropriate solvent in casting solution to achieve high water flux and BSA rejection. They prepared membrane pore size between 5 and 10 nm and the pure water flux was 1.16–14.65 L m^{-2} h^{-1} bar^{-1} when the PES content was between 16% and 24% [59]. In our formulas, 23 wt.% of PES and 16 wt.% of PVP dissolved in DMAc. Such excellent water and flux rejection performance could be due to the two reasons, one is that the average interdiffusion coefficient of DMAc-water system is higher than that of NMP-water system. By increasing the diffusion rate between solvent and non-solvent, instant desorption can be achieved, thereby increasing the porosity of the top and support layer [12]. Another is that the high concentration of PVP increases the viscosity of the casting solution resulting in the reduction of solvent and non-solvent exchange rate and delayed demixing occurred. Consequently, a membrane would be formed with less finger-like pore and lower mean pore size.

When the MoS_2 was introduced into the formula, the pure water flux increased from 76.16 to 84.41 L m^{-2} h^{-1} bar^{-1}, while the PEG 10 kDa rejection decreased from 93.28% to 91.72%, which was the result of the increased pore size in the M1 membrane. The increased pore size can be attributed to the domination of thermodynamic features when the content of MoS_2 was below an optimum concentration. Compare to the M1, when the content of MoS_2 sheets was 2.5–5.0 wt.%, the water flux reduced, which was due to the increased load of MoS_2, the main viscosity effect in the polymer solution was generated, resulting in dense, and less porosity of the membrane. This can be due to the domination of rheological features [50]. When the concentration of MoS_2 was between 2.5 and 4.0wt.%, the modified TUF membranes showed 8.84% to 11.25% higher water flux than the pristine membrane. Moreover, the modified membranes have a better PEG rejection property compared to the M0 membrane. These results indicated that moderated MoS_2 broke the trade-off between the permeability and rejection property of membranes, and comprehensively improved the separation performance of TUF membranes. The major reason for this result was based on the increased number of transfer channels in PES/MoS_2 matrix. The steric hindrance and electrostatics affect the dispersion of nanoparticles and the pore channels [60–62]. An appropriate amount of MoS_2 showed a well distribution in the polymer matrix, and this brought more effective water channels. However, when the content of MoS_2 sheets was 5.0 wt.%, the water flux reduced, which was due to the declined hydrophilic nature and porosity of the membranes. In the M5 membrane, an excessive dose of MoS_2 sheets in the membrane played as a hindrance to the passage of water molecules. As shown in Fig. 1e (M5), a further increase of MoS_2 resulted in a relatively serious aggregation, leading to more irregular combinations and permutations of MoS_2 near the skin layer in the membrane. The above results indicated that by optimizing the concentration of MoS_2 in the casting solution, the filtration performance of TUF membrane can be effectively enhanced. Table 2 summarizes the water flux of the PES/MoS_2 membranes and other TUF membranes with similar MWCO. The result indicated that the PES/MoS_2 membranes fabricated in this study show higher water flux than other TUF membranes.

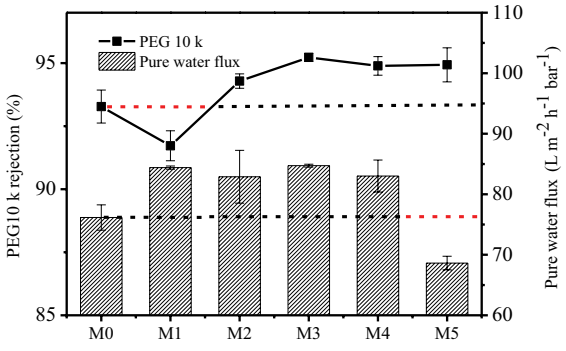

Fig. 8. Pure water flux and PEG 10 kDa rejection of membranes.

Considering the blending with inorganic material and a polymer matrix, it is necessary to evaluate the loss of MoS_2 nanosheets from mixed matrix membrane in a dynamic condition. A long-term filtration was carried out to assess the loss of MoS_2 from the M3 membrane. The standard curve Fig. 9a shows that the optical absorbance of MoS_2 after background subtraction scaled linearly with the different MoS_2 concentrations in water. Fig. 9b shows that the concentration of MoS_2 in both permeated water and concentrated water is quite low. The result showed that MoS_2 was relatively stable in the PES matrix.

To evaluate the rejection performance of the membranes rose bengal (estimated size: 1.45 nm) [72] and direct red 80 (estimated size: 3.91 nm) [73] were selected as the sample dyes for further investigating the rejection property of fabricated TUF membranes. Results in Fig. 10a indicates that all the prepared membranes had excellent separation performances of rose bengal at 10 mg L^{-1}. With the increase of rose bengal concentration from 10 to 100 mg L^{-1}, the membrane removal efficiency was significantly reduced.

Table 2
Comparison of water flux, MWCO, and pore size of PES/MOS_2 membranes with literature reported TUF membranes

Membranes	Water flux (L m^{-2} h^{-1} bar^{-1})	MWCO/pore size	Reference
PES/MoS_2	68.6–84.7	8.7–9.8 kDa (3.45–3.71 nm)	This work
PES-9	37.5	9.0 kDa	[63]
PES-6	15.0	6.0 kDa	[64]
PES 20	12.0	10.0 kDa	[65]
PES	2.5–5.2	4.53–5.13 nm	[12]
PES-TiO_2	0.7–1.44	2.0–2.9 nm	[21]
PES-TiO_2-MWCNTs	0.74–1.13	2.17 nm	[22]
Polyamide	21.3	8.0 kDa	[66]
Regenerated cellulose	35.8	10.0 kDa	[66]
PLGC	21.67	10.0[a] kDa	[67]
PAEK-COOH	29.5	9.3 kDa	[68]
MT68	16.7	8.0 kDa	[69]
FS10	37.5–40.0	6.0–8.0 kDa	[70]
PAN/SiO_2-25	58.7	6.0 kDa	[71]

[a]Information supplied by Millipore.

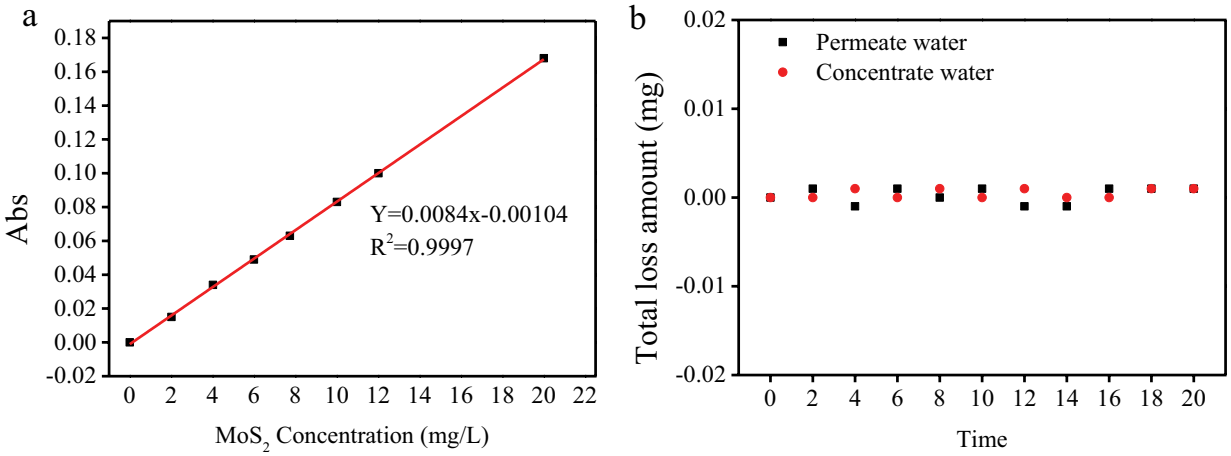

Fig. 9. Absorbance of different concentrations of MoS_2 of dispersed in DI water under 674 nm wavelength (a) and total loss amount of MoS_2 on M3 with time during operation (b) (pure water is the feed water and the operation press is 1.0 bar).

This was possibly due to the increase in impurities (i.e., Cl^-, SO_4^{2-}, and HCO_3^-) as the dye concentration increase. The increasing of these ionic can intensify the electrostatic shielding, thus reduced the rejection of rose bengal [74]. Specifically, when the concentration of rose bengal was 100 mg L^{-1}, the variation trend of dye retention rate was closely related to the pore size of membranes. The pore size of the M1 membrane was 3.87 nm which was larger than that of the M0 membrane (3.58 nm), therefore the rose bengal rejection reduced from 83.29% to 79.93%. When the concentration of MoS_2 sheets was between 2.5 and 4.0 wt.%, the rejection performance of modified TUF membranes increased gradually due to the decreasing membrane pore size. The results indicated that 3.0 wt.% MoS_2 modified TUF membranes showed improved rejection property of rose bengal from 79.93% to 91.60%. Fig. 10b shows that all the prepared membranes had excellent separation performances of direct red 80 in every different concentration. When the concentration was 100 mg L^{-1}, the rejection of the M0 membrane was 99.60% and M3 was 99.89%. This further confirmed that the pore diameter of all modified membranes were smaller than the size of direct red 80. The rose bengal concentration reduce the rejection of the membrane obviously because the size of the rose bengal is smaller than the membrane pore size, and might lead to adsorptive fouling. Considering adsorptive fouling that may occur during membrane separation, a higher initial feed concentration (50 mg L^{-1}) was introduced to compare the membrane flux changes of the M0 and M3 membranes. Figs. 10c and d show that M3 membrane experienced a further flux decline and the permeation of rose Bengal dropped faster than direct red 80.

Fig. 11a shows that the permeation flux of M0 and M3 decreased gradually with feed solution changing from pure

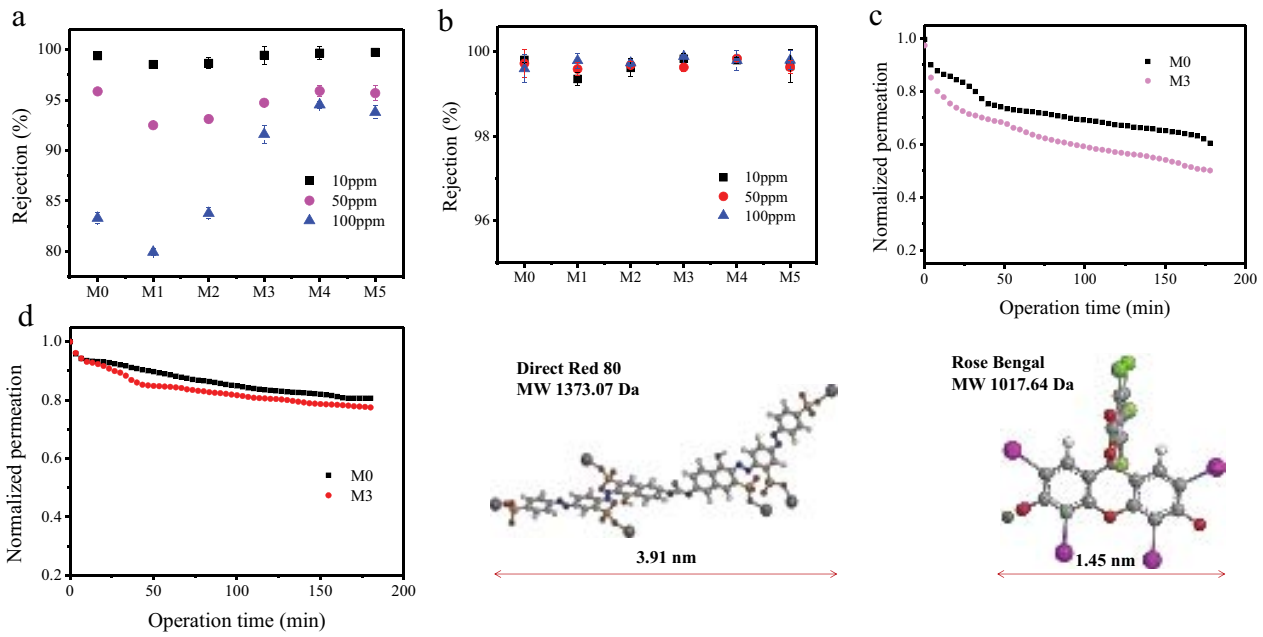

Fig. 10. Influence of initial feed concentration on rose bengal rejection (a), and direct red 80 rejection (b) and water decease of M0 and M3 (c) for rose bengal and (d) for direct red 80.

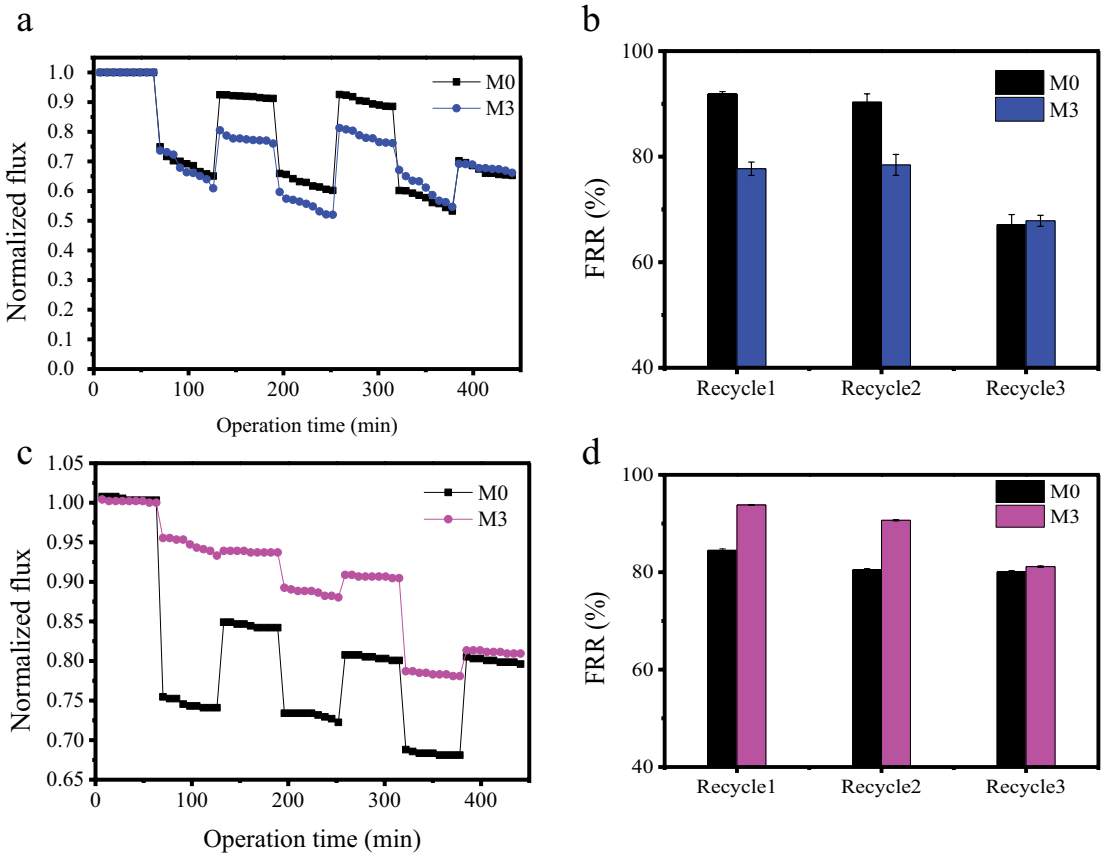

Fig. 11. Normalized flux (J_w/J_{w0}) and FRR of M0 and M3 with fouling and cleaning cycles (1.0 g L^{-1} PEG, 0.1 bar) (a and b), normalized flux (J_w/J_{w0}) and FRR of M0 and M3 with fouling and cleaning cycles (50 mg L^{-1} rose bengal, 0.1 bar) (c and d).

water to PEG 10 kDa solution. This due to the PEG 10 kD linear molecule blocked in the membrane pores or trapped on the membrane surface. Therefore, the membranes cannot be recovered to their original water flux value after circulating filtration. In addition, the normalized permeation of the M0 was higher than that of the M3 in the first cycle. The normalized permeation of the M3 was equal to that of M0 in the third cycle, this was mainly because of their different membrane roughness and hydrophilicity. Fig. 11b shows that the FRR decreased from 91.87% of M0 to 77.71% of M3. This indicated that M0 had better PEG antifouling performance than M3 due to the hydrophilic surface. Fig. 11c reveals the rose Bengal dye normalized permeation flux of M0 and M3. In the first two cycles, the normalized permeation of the M0 decreased faster than M3. However, after cleaning, M3 restored better. In the third cycle, both M0 and M3 have similar normalized permeation values. In addition, the FRR of M0 decreased from 84.50% of the first cycle to 80.01% of the third cycle. While Fig. 11d shows that FRR of the M3 decreased from 93.81% of the first cycle to 81.14% of the third cycle. This mainly because of the adsorption fouling of the rose Bengal dye molecule in the membrane surface and pores. The result indicated that further study on the improvement of the anti-fouling property of 2D MoS_2 modified TUF membranes was critical.

4. Conclusion

In this work, MoS_2 sheets were blended into the PES matrix to fabricate PES/MoS_2 mixed matrix TUF membranes. The results revealed that MoS_2 sheets impacted the structure and properties of TUF membranes by facilitating the growth of finger-like macro voids and controlling the membrane pore size. Moreover, compared with the pristine membrane, the PES/MoS_2 membranes showed improvements in both the water flux and the PEG (10 kDa) rejection property, when the concentrations of MoS_2 was between 2.5 and 4.0 wt.%, which overcomes the typical trade-off phenomenon in membranes. The as-prepared membrane also showed excellent separation performance for rose bengal and direct red 80. Therefore, the PES/MoS_2 mixed matrix membrane presents an effective approach to coordinate the "trade-off" effect of mixed matrix membranes. Specifically, the MoS_2 sheets applied in this study was commercial grade, without further time-consuming modification. Therefore, this study also provides a method of high-quality TUF membranes which is facile and can be easily applied in industrial membrane fabrication producing.

Acknowledgments

This work was supported by grants from the National Key R&D Program of China (2018YFC1903205), the Bureau of Frontier Sciences and Education (QYZDB-SSW-DQC044), the Bureau of International Cooperation (132C35KYSB20160018), the Chinese Academy of Sciences, and the Joint Project between CAS-CSIRO (132C35KYSB20170051). The authors thank Mrs. Temitope Fausat Ajibade for grammatical revision, Mr. Yi Li for drawing the dye structure diagram, the technical help from Hongyun Ren for microtome specimen of Membranes in the TEM measurement and Cuihui Cao for tensile testing. The authors also acknowledge Dr. Olusegun K. Abass, Dr. Qing liang Jiang, Ms. Shishi Yang, and Dr. Fang Fang for their assistance in the membrane preparation.

References

[1] R.W. Baker, Membrane Technology and Applications, 3rd ed., John Wiley & Sons, Newark, California, USA, 2012, pp. 253–300.
[2] O.S. Odegaard H, Melin E, Eikebrokk B, NOM removal technologies - Norwegian experiences, Drink. Water Eng. Sci., 3 (2010) 1–9.
[3] N. Lee, G. Amy, J.P. Croue, H. Buisson, Identification and understanding of fouling in low-pressure membrane (MF/UF) filtration by natural organic matter (NOM), Water Res., 38 (2004) 4511–4523.
[4] Y. Xu, C. Chen, X. Li, J. Lin, Y. Liao, Z. Jin, Recovery of humic substances from leachate nanofiltration concentrate by a two-stage process of tight ultrafiltration membrane, J. Cleaner Prod., 161 (2017) 84–94.
[5] J. Winter, B. Barbeau, P. Berube, Nanofiltration and tight ultrafiltration membranes for natural organic matter removal-contribution of fouling and concentration polarization to filtration resistance, Membranes, 7 (2017) 1–14.
[6] Y.D. Xu, D.B. Yue, Y. Zhu, Y.F. Nie, Fractionation of dissolved organic matter in mature landfill leachate and its recycling by ultrafiltration and evaporation combined processes, Chemosphere, 64 (2006) 903–911.
[7] C. Conidi, R. Mazzei, A. Cassano, L. Giorno, Integrated membrane system for the production of phytotherapics from olive mill wastewaters, J. Membr. Sci., 454 (2014) 322–329.
[8] C.M. Galanakis, R. Castro-Muñoz, A. Cassano, C. Conidi, Recovery of High-Added-Value Compounds from Food Waste by Membrane Technology, A. Figoli, A. Cassano, A. Basile, Eds., Membrane Technologies for Biorefining, Elsevier, UK, 2016, pp. 189–215.
[9] J. Lin, W. Ye, M.-C. Baltaru, Y.P. Tang, N.J. Bernstein, P. Gao, S. Balta, M. Vlad, A. Volodin, A. Sotto, P. Luis, A.L. Zydney, B. Van der Bruggen, Tight ultrafiltration membranes for enhanced separation of dyes and Na_2SO_4 during textile wastewater treatment, J. Membr. Sci., 514 (2016) 217–228.
[10] G. Jiang, S. Zhang, Y. Zhu, S. Gao, H. Jin, L. Luo, F. Zhang, J. Jin, Hydrogel-embedded tight ultrafiltration membrane with superior anti-dye-fouling property for low-pressure driven molecule separation, J. Mater. Chem. A, 6 (2018) 2927–2934.
[11] A.L. Ahmad, A.A. Abdulkarim, B.S. Ooi, S. Ismail, Recent development in additives modifications of polyethersulfone membrane for flux enhancement, Chem. Eng. J., 223 (2013) 246–267.
[12] M.A. Alaei Shahmirzadi, S.S. Hosseini, G. Ruan, N.R. Tan, Tailoring PES nanofiltration membranes through systematic investigations of prominent design, fabrication and operational parameters, RSC Adv., 5 (2015) 49080–49097.
[13] A. Rahimpour, M. Jahanshahi, S. Khalili, A. Mollahosseini, A. Zirepour, B. Rajaeian, Novel functionalized carbon nanotubes for improving the surface properties and performance of polyethersulfone (PES) membrane, Desalination, 286 (2012) 99–107.
[14] N.A. Alenazi, M.A. Hussein, K.A. Alamry, A.M. Asiri, Modified polyether-sulfone membrane: a mini review, Des. Monomers Polym., 20 (2017) 532–546.
[15] A.L. Ahmad, W.Y. Pang, Z.M.H. Mohd Shafie, N.D. Zaulkiflee, PES/PVP/TiO_2 mixed matrix hollow fiber membrane with antifouling properties for humic acid removal, J. Water Process Eng., 31 (2019) 1–9, doi: 10.1016/j.jwpe.2019.100827.
[16] W.Y. Pang, A.L. Ahmad, N.D. Zaulkiflee, Antifouling and antibacterial evaluation of ZnO/MWCNT dual nanofiller polyethersulfone mixed matrix membrane, J. Environ. Manage., 249 (2019) 1–10, doi: 10.1016/j.jenvman.2019.109358.
[17] P.S. Goh, B.C. Ng, W.J. Lau, A.F. Ismail, Inorganic nanomaterials in polymeric ultrafiltration membranes for water treatment, Sep. Purif. Rev., 44 (2014) 216–249.
[18] M.R. Mehrnia, Y.M. Mojtahedi, M. Homayoonfal, What is the concentration threshold of nanoparticles within the membrane

structure? A case study of Al_2O_3/PSf nanocomposite membrane, Desalination, 372 (2015) 75–88.
[19] M. Zhang, K. Zhang, B. De Gusseme, W. Verstraete, Biogenic silver nanoparticles (bio-Ag^0) decrease biofouling of bio-Ag^0/PES nanocomposite membranes, Water Res., 46 (2012) 2077–2087.
[20] E. Celik, H. Park, H. Choi, Carbon nanotube blended polyethersulfone membranes for fouling control in water treatment, Water Res., 45 (2011) 274–282.
[21] V. Vatanpour, S.S. Madaeni, A.R. Khataee, E. Salehi, S. Zinadini, H.A. Monfared, TiO_2 embedded mixed matrix PES nanocomposite membranes: influence of different sizes and types of nanoparticles on antifouling and performance, Desalination, 292 (2012) 19–29.
[22] V. Vatanpour, S.S. Madaeni, R. Moradian, S. Zinadini, B. Astinchap, Novel antibifouling nanofiltration polyethersulfone membrane fabricated from embedding TiO_2 coated multiwalled carbon nanotubes, Sep. Purif. Technol., 90 (2012) 69–82.
[23] S. Zinadini, A.A. Zinatizadeh, M. Rahimi, V. Vatanpour, H. Zangeneh, Preparation of a novel antifouling mixed matrix PES membrane by embedding graphene oxide nanoplates, J. Membr. Sci., 453 (2014) 292–301.
[24] Z. Chu, K. Chen, C. Xiao, H. Ling, Z. Hu, Performance improvement of polyethersulfone ultrafiltration membrane containing variform inorganic nano-additives, Polymer, 188 (2020) 1–11, doi: 10.1016/j.polymer.2020.122160.
[25] R. Ganatra, Q. Zhang, Few-layer MoS_2: a promising layered semiconductor, ACS Nano, 8 (2014) 4074–4099.
[26] D. Wang, Z. Wang, L. Wang, L. Hu, J. Jin, Ultrathin membranes of single-layered MoS_2 nanosheets for high-permeance hydrogen separation, Nanoscale, 7 (2015) 17649–17652.
[27] M. Heiranian, A.B. Farimani, N.R. Aluru, Water desalination with a single-layer MoS_2 nanopore, Nat. Commun., 6 (2015) 1–5.
[28] M. Deng, K. Kwac, M. Li, Y. Jung, H.G. Park, Stability, molecular sieving, and ion diffusion selectivity of a lamellar membrane from two-dimensional molybdenum disulfide, Nano Lett., 17 (2017) 2342–2348.
[29] J. Kou, J. Yao, L. Wu, X. Zhou, H. Lu, F. Wu, J. Fan, Nanoporous two-dimensional MoS_2 membranes for fast saline solution purification, Phys. Chem. Chem. Phys., 18 (2016) 22210–22216.
[30] P. Zhang, J.-L. Gong, G.-M. Zeng, B. Song, W. Cao, H.-Y. Liu, S.-Y. Huan, P. Peng, Novel "loose" GO/MoS_2 composites membranes with enhanced permeability for effective salts and dyes rejection at low pressure, J. Membr. Sci., 574 (2019) 112–123.
[31] Z. Wang, B. Mi, Environmental applications of 2D molybdenum disulfide (MoS_2) nanosheets, Environ. Sci. Technol., 51 (2017) 8229–8244.
[32] S. Yang, K. Zhang, Few-layers MoS_2 nanosheets modified thin film composite nanofiltration membranes with improved separation performance, J. Membr. Sci., 595 (2020) 1–11, doi: 10.1016/j.memsci.2019.117526.
[33] M.-Q. Ma, C. Zhang, C.-Y. Zhu, S. Huang, J. Yang, Z.-K. Xu, Nanocomposite membranes embedded with functionalized MoS_2 nanosheets for enhanced interfacial compatibility and nanofiltration performance, J. Membr. Sci., 591 (2019) 1–8, doi: 10.1016/j.memsci.2019.117316.
[34] F.A. Pacheco, I. Pinnau, M. Reinhard, J.O. Leckie, Characterization of isolated polyamide thin films of RO and NF membranes using novel TEM techniques, J. Membr. Sci., 358 (2010) 51–59.
[35] J.P. Cerisuelo, R. Gavara, P. Hernández-Muñoz, Diffusion modeling in polymer–clay nanocomposites for food packaging applications through finite element analysis of TEM images, J. Membr. Sci., 482 (2015) 92–102.
[36] K. Wang, X. Lin, G. Jiang, J.Z. Liu, L. Jiang, C.M. Doherty, A.J. Hill, T. Xu, H. Wang, Slow hydrophobic hydration induced polymer ultrafiltration membranes with high water flux, J. Membr. Sci., 471 (2014) 27–34.
[37] D. Dolar, K. Kosutic, T. Strmecky, Hybrid processes for treatment of landfill leachate: coagulation/UF/NF-RO and adsorption/UF/NF-RO, Sep. Purif. Technol., 168 (2016) 39–46.
[38] C. Liu, H. Mao, J. Zheng, S. Zhang, *In situ* surface crosslinked tight ultrafiltration membrane prepared by one-step chemical reaction-involved phase inversion process between activated PAEK-COOH and PEI, J. Membr. Sci., 538 (2017) 58–67.
[39] S. Singh, K.C. Khulbe, T. Matsuura, P. Ramamurthy, Membrane characterization by solute transport and atomic force microscopy, J. Membr. Sci., 142 (1998) 111–127.
[40] Y. Li, E. Wong, Z. Mai, B. Van der Bruggen, Fabrication of composite polyamide/Kevlar aramid nanofiber nanofiltration membranes with high permselectivity in water desalination, J. Membr. Sci., 592 (2019) 1–11, doi: 10.1016/j.memsci.2019.117396.
[41] M. Zhang, R.W. Field, K. Zhang, Biogenic silver nanocomposite polyethersulfone UF membranes with antifouling properties, J. Membr. Sci., 471 (2014) 274–284.
[42] S. Wang, H. Yu, H. Zhang, A. Wang, M. Zhao, Y. Chen, L. Mei, J. Wang, Broadband few-layer MoS_2 saturable absorbers, Adv. Mater., 26 (2014) 3538–3544.
[43] R. Hickey, Processes for Bioconverting Syngas to Oxygenated Hydrocarbonaceous Compounds, Synata Bio Inc., 2018.
[44] R. Jamshidi Gohari, E. Halakoo, N.A.M. Nazri, W.J. Lau, T. Matsuura, A.F. Ismail, Improving performance and antifouling capability of PES UF membranes via blending with highly hydrophilic hydrous manganese dioxide nanoparticles, Desalination, 335 (2014) 87–95.
[45] J. Zheng, H. Zhang, S. Dong, Y. Liu, C.T. Nai, H.S. Shin, H.Y. Jeong, B. Liu, K.P. Loh, High yield exfoliation of two-dimensional chalcogenides using sodium naphthalenide, Nat. Commun., 5 (2014) 1–7, doi: 10.1038/ncomms3995.
[46] M. Saraswathi, D. Rana, A. Nagendran, S. Alwarappan, Custom-made PEI/exfoliated-MoS_2 nanocomposite ultrafiltration membranes for separation of bovine serum albumin and humic acid, Mater. Sci. Eng., C, 83 (2018) 108–114.
[47] I. Cabasso, E. Klein, J.K. Smith, Polysulfone hollow fibers. II. Morphology, J. Appl. Polym. Sci., 21 (1977) 165–180.
[48] A.F. Ismail, A.R. Hassan, Effect of additive contents on the performances and structural properties of asymmetric polyethersulfone (PES) nanofiltration membranes, Sep. Purif. Technol., 55 (2007) 98–109.
[49] Y.-n. Yang, W. Jun, Z. Qing-zhu, C. Xue-si, Z. Hui-xuan, The research of rheology and thermodynamics of organic–inorganic hybrid membrane during the membrane formation, J. Membr. Sci., 311 (2008) 200–207.
[50] S. Arefi-Oskoui, A. Khataee, M. Safarpour, V. Vatanpour, Modification of polyethersulfone ultrafiltration membrane using ultrasonic-assisted functionalized MoS_2 for treatment of oil refinery wastewater, Sep. Purif. Technol., 238 (2020) 1–13, doi: 10.1016/j.seppur.2019.116495.
[51] X. Feng, X. Wang, W. Xing, K. Zhou, L. Song, Y. Hu, Liquid-exfoliated MoS_2 by chitosan and enhanced mechanical and thermal properties of chitosan/MoS_2 composites, Compos. Sci. Technol., 93 (2014) 76–82.
[52] N.N. Gumbi, M. Hu, B.B. Mamba, J. Li, E.N. Nxumalo, Macrovoid-free PES/SPSf/O-MWCNT ultrafiltration membranes with improved mechanical strength, antifouling and antibacterial properties, J. Membr. Sci., 566 (2018) 288–300.
[53] S. Wu, Z. Wang, S. Xiong, Y. Wang, Tailoring TiO_2 membranes for nanofiltration and tight ultrafiltration by leveraging molecular layer deposition and crystallization, J. Membr. Sci., 578 (2019) 149–155.
[54] I.-C. Kim, H.-G. Yun, K.-H. Lee, Preparation of asymmetric polyacrylonitrile membrane with small pore size by phase inversion and post-treatment process, J. Membr. Sci., 463 (2002) 145–165.
[55] M. Gholami, S. Nasseri, C.Y. Feng, T. Matsuura, K.C. Khulbe, The effect of heat-treatment on the ultrafiltration performance of polyethersulfone (PES) hollow-fiber membranes, Desalination, 155 (20003) 293–301.
[56] Y. Song, Z. Jiang, B. Gao, H. Wang, M. Wang, Z. He, X. Cao, F. Pan, Embedding hydrophobic MoS_2 nanosheets within hydrophilic sodium alginate membrane for enhanced ethanol dehydration, Chem. Eng. Sci., 185 (2018) 231–242.
[57] M. Sri Abirami Saraswathi, D. Rana, J.S. Beril Melbiah, D. Mohan, A. Nagendran, Effective removal of bovine serum

albumin and humic acid contaminants using poly (amide imide) nanocomposite ultrafiltration membranes tailored with GO and MoS_2 nanosheets, Mater. Chem. Phys., 216 (2018) 170–176.
[58] X. Cui, X. Wu, J. Zhang, J. Wang, H. Zhang, F. Du, L. Qu, X. Cao, P. Zhang, A loosely stacked lamellar membrane of irregular MoS_2 flakes for ultrahigh water and organics permeation, J. Mater. Chem. A, 7 (2019) 12698–12705.
[59] S. Alibakhshi, M. Youssefi, S.S. Hosseini, A. Zadhoush, Tuning morphology and transport in ultrafiltration membranes derived from polyethersulfone through exploration of dope formulation and characteristics, Mater. Res. Exp., 6 (2019) 1–14, doi: 10.1088/2053-1591/ab56c3.
[60] G. Zhang, M. Zhou, Z. Xu, C. Jiang, C. Shen, Q. Meng, Guanidyl-functionalized graphene/polysulfone mixed matrix ultrafiltration membrane with superior permselective, antifouling and antibacterial properties for water treatment, J. Colloid Interface Sci., 540 (2019) 295–305.
[61] Q. Yang, X. Li, L. Zhang, G. Wang, G. Chen, D. Lin, B. Xing, Dispersion and stability of multi-walled carbon nanotubes in water as affected by humic acids, J. Mol. Liq., 279 (2019) 361–369.
[62] M. Madkour, A. Bumajdad, F. Al-Sagheer, To what extent do polymeric stabilizers affect nanoparticles characteristics?, Adv. Colloid Interface Sci., 270 (2019) 38–53.
[63] A.V.R. Reddy, D.J. Mohan, A. Bhattacharya, V.J. Shah, P.K. Ghosh, Surface modification of ultrafiltration membranes by preadsorption of a negatively charged polymer_ I. Permeation of water soluble polymers and inorganic salt solutions and fouling resistance properties, J. Membr. Sci., 214 (2003) 211–221.
[64] S. Guo, J. Luo, Y. Wu, B. Qi, X. Chen, Y. Wan, Decoloration of sugarcane molasses by tight ultrafiltration: filtration behavior and fouling control, Sep. Purif. Technol., 204 (2018) 66–74.
[65] S. Al Aani, C.J. Wright, N. Hilal, Investigation of UF membranes fouling and potentials as pre-treatment step in desalination and surface water applications, Desalination, 432 (2018) 115–127.
[66] N. Park, Y. Lee, S. Lee, J. Cho, Removal of taste and odor model compound (2,4,6-trichloroanisole) by tight ultrafiltration membranes, Desalination, 212 (2007) 28–36.
[67] A.I. Schäfer, A.G. Fane, T.D. Waite, Cost factors and chemical pretreatment effects in the membrane filtration of waters containing natural organic matter, Water Res., 35 (2001) 1509–1517.
[68] C. Liu, H. Mao, J. Zheng, S. Zhang, Tight ultrafiltration membrane: preparation and characterization of thermally resistant carboxylated cardo poly (arylene ether ketone)s (PAEK-COOH) tight ultrafiltration membrane for dye removal, J. Membr. Sci., 530 (2017) 1–10.
[69] L. Vandanjon, R. Johannsson, M. Derouiniot, P. Bourseau, P. Jaouen, Concentration and purification of blue whiting peptide hydrolysates by membrane processes, J. Food Eng., 83 (2007) 581–589.
[70] R. Atra, G. Vatai, E. Bekassy-Molnar, A. Balint, Investigation of ultra- and nanofiltration for utilization of whey protein and lactose, J. Food Eng., 67 (2005) 325–332.
[71] Y. Hu, Z. Lü, C. Wei, S. Yu, M. Liu, C. Gao, Separation and antifouling properties of hydrolyzed PAN hybrid membranes prepared via *in-situ* sol–gel SiO_2 nanoparticles growth, J. Membr. Sci., 545 (2018) 250–258.
[72] B.Y. Guo, S.D. Jiang, M.J. Tang, K. Li, S. Sun, P.Y. Chen, S. Zhang, MoS_2 membranes for organic solvent nanofiltration: stability and structural control, J. Phys. Chem. Lett., 10 (2019) 4609–4617.
[73] I. Gadwal, G. Sheng, R.L. Thankamony, Y. Liu, H. Li, Z. Lai, Synthesis of sub-10 nm two-dimensional covalent organic thin film with sharp molecular sieving nanofiltration, ACS Appl. Mater. Interface, 10 (2018) 12295–12299.
[74] M. Jiang, K. Ye, J. Deng, J. Lin, W. Ye, S. Zhao, B. Van der Bruggen, Conventional ultrafiltration as effective strategy for dye/salt fractionation in textile wastewater treatment, Environ. Sci. Technol., 52 (2018) 10698–10708.